Modeling of Shear-Critical Reinforced Concrete Structures Repaired with Fiber-Reinforced Polymer Composites

Sang-Woo Kim[1] and Frank J. Vecchio[2]

Abstract: This paper describes a study in which finite-element (FE) analysis procedures were used to predict the behavior of a reinforced concrete (RC) frame shear strengthened with fiber-reinforced polymer (FRP) composites. Details are presented of the numerical techniques used to represent the RC frame, the FRP, and the bond properties between the FRP and the concrete. The FE analysis is performed using a two-dimensional nonlinear FE analysis program based on the disturbed stress field model. To augment verification studies undertaken with beam specimens previously tested, a large-scale RC frame with one-span and two-story height was constructed and tested under lateral load conditions. The frame was first heavily damaged in shear, repaired with FRP wrap, and then subjected to a regime of reversed cyclic loads. A detailed comparison is carried out between analytical and experimental results for the hysteretic response, damage mode, crack pattern, and deformation of the frame. It is concluded that reasonably accurate simulations of the behavior of FRP-repaired shear-critical structures can be achieved through finite-element modeling.

DOI: 10.1061/(ASCE)0733-9445(2008)134:8(1288)

CE Database subject headings: Concrete, reinforced; Concrete structures; Shear; Finite element method; Fiber reinforced polymers.

Introduction

There still exist, in many locales, reinforced concrete (RC) structures that were either built at a time when effective design provisions for lateral loads were not yet established or were built in breach of governing standards or practice. An example of such a structure is a cement plant preheater tower built in a seismically active country of Central America, as seen in Fig. 1. Although the tower was erected in the late 1990s, it was based on design concepts developed approximately 30 to 40 years ago; similar towers exist in a number of places around the world. Due to various design deficiencies relative to current code requirements, the behavior of this and similar structures under lateral load conditions is governed by shear failure mechanisms. For economic and environmental reasons, it would be too costly to tear down and rebuild these structures to allay safety concerns. In the case of the cement preheater tower, the economic loss from an extended stoppage in plant production would far exceed the cost of demolition and reconstruction. Accordingly, it is often more expedient to repair and strengthen such structures to extend their life cycles.

In recent years, fiber-reinforced polymer (FRP) composites are being widely used for strengthening RC structures in flexure and shear. FRP materials have a high strength-to-weight ratio and a high corrosion resistance as well as nonmagnetic and nonconductive properties, in comparison to steel plates also used for strengthening. The high strength-to-weight ratio, in particular, leads to not only great ease in site handling but also reducing labor cost.

In the early 1980s, the FRP-strengthening technique was first developed in Germany and Switzerland (Triantafillou 1998). Studies on flexural and shear strengthening with FRP composites were first carried out by Saadatmanesh and Ehsani (1990) and Berset (1992), respectively. Most research studies on shear strengthening of RC members performed before 2000 were focused on the shear strength enhancement due to the geometric and mechanical properties of the FRP composite (Al-Sulaimani et al. 1994; Chajes et al. 1995; Norris et al. 1997; Chaallal et al. 1998). Recently, however, many researchers have studied other parameters contributing to the shear resistance of the FRP shear-strengthened RC members (Li et al. 2001; Pellegrino and Modena 2002, 2006; Bousselham and Chaallal 2004, 2006). For example, the contributions of the concrete, the longitudinal and transverse reinforcement, and the geometry of RC member (e.g., shear span-to-depth ratio and size effect) are among the parameters examined. Several researchers have also proposed design methods, based on the effective FRP strain, to estimate the shear strength of RC beams strengthened in shear with FRP composites (Khalifa 1998; Triantafillou 1998; Triantafillou and Antonopoulos 2000; Chen and Teng 2003).

A review of published related research reveal that most studies on the shear strengthening with FRP composites are mainly focused on the evaluation of the shear strength enhancement of the FRP-strengthened RC members for shear, based on empirical methods. This is because the failure mechanism of RC members strengthened in shear with FRP laminates varies and is complex. It would, thus, be desirable to have an analytical approach, satisfying both equilibrium and compatibility relationships, to model the response of the RC structures strengthened with FRP composites. However, the literature also indicated that not only are finite-element (FE)-based assessment methods for shear strengthening

[1]Senior Researcher, Dept. of Architectural Engineering, Sungkyunkwan Univ., 300 Cheoncheon-dong, Jangan-gu, Suwon 440-746, South Korea (corresponding author). E-mail: swkim91@skku.edu

[2]Professor, Dept. of Civil Engineering, 35 St. George St., Univ. of Toronto, Toronto, ON, M5S-1A4, Canada. E-mail: fjv@civ.utoronto.ca

Note. Associate Editor: Enrico Spacone. Discussion open until January 1, 2009. Separate discussions must be submitted for individual papers. To extend the closing date by one month, a written request must be filed with the ASCE Managing Editor. The manuscript for this paper was submitted for review and possible publication on June 15, 2007; approved on November 1, 2007. This paper is part of the ***Journal of Structural Engineering***, Vol. 134, No. 8, August 1, 2008. ©ASCE, ISSN 0733-9445/2008/8-1288–1299/$25.00.

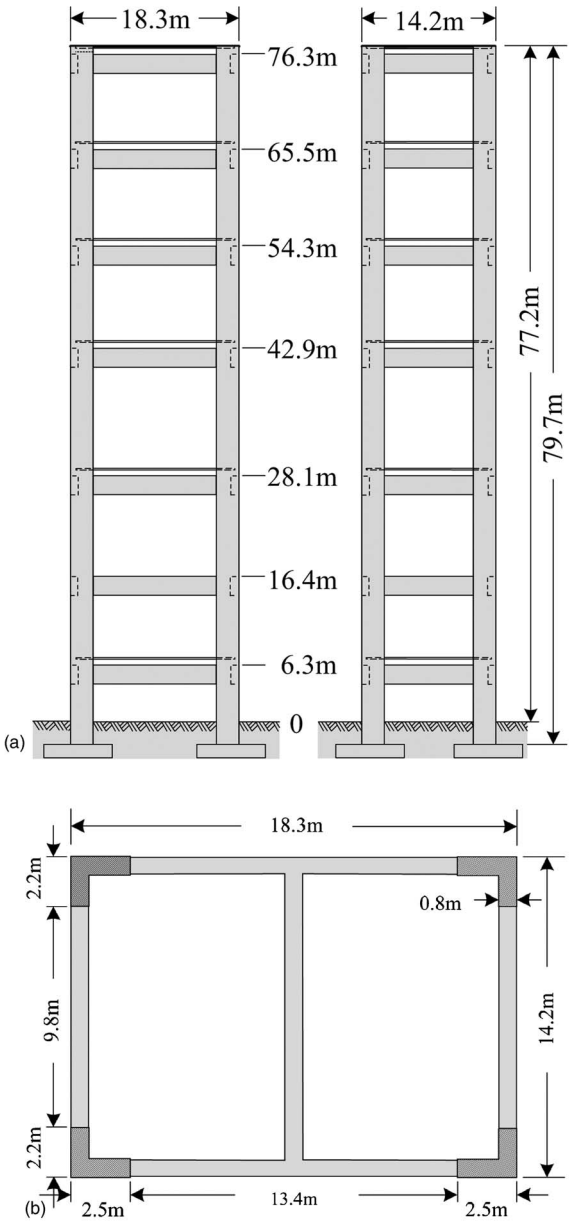

Fig. 1. Typical structural layout of cement plant preheater tower: (a) elevation; (b) floor plan

with FRP composites rare, but also no attempt has yet been reported for the FE analysis of the shear-critical RC frames strengthened with FRP composites.

The disturbed stress field model (DSFM) (Vecchio 2000) was recently developed to better model the shear behavior of the RC structures. The DSFM extended the equilibrium, compatibility, and constitutive response formulations of the modified compression field theory (MCFT) (Vecchio and Collins 1986) by, among other things, taking into account shear slip deformations on crack surfaces. Therefore, it combines aspects of both the rotating and the fixed crack models. That is, in the DSFM, the directions of principal stresses may differ from those of principal strains, while still permitting the reorientation of the concrete principal stress direction and crack direction. This model has been used to describe the nonlinear shear response of RC structures through its implementation in a nonlinear FE analysis program (VecTor2). Recently, the DSFM was successfully used to analyze the

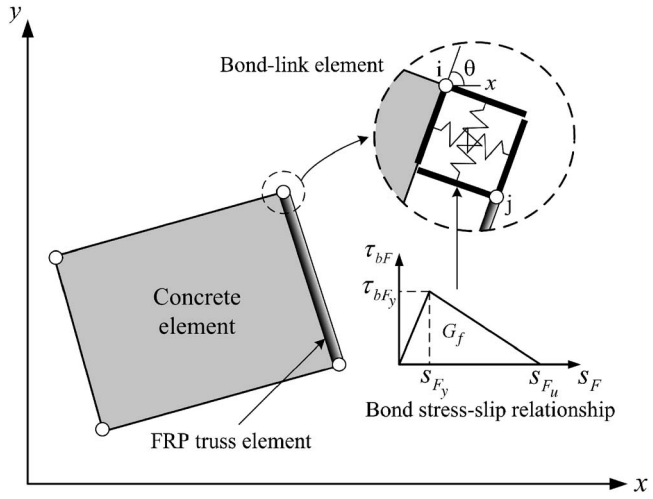

Fig. 2. Representation of FRP truss and bond-link elements

RC beams shear strengthened with FRP composites (Sato and Vecchio 2003).

This paper presents material and structural modeling concepts that enable the use of FE-based methods for the analysis of RC frames shear strengthened with FRP composites acting under lateral reversed cyclic loads. According to the proposed modeling methods, a nonlinear FE analysis is performed to evaluate the response of a previously tested one-span two-story shear-critical RC frame. Applicability of the DSFM as an analysis tool for frames strengthened in shear with FRP laminates is verified by comparing theoretical and experimental results.

FE Modeling of FRP-Repaired Structures

Representation of FRP Composite

In this study, "tension-only" truss elements were used in FE modeling to represent the FRP composites. As shown in Fig. 2, the truss element representing the FRP composite is connected to a concrete element via a bond-link element. The FRP truss element consists of two nodes with two degrees of freedom per node and thus has a total of four degrees of freedom. It is able to assume any orientation in the *x*-*y* coordinate system, has a uniform cross-sectional area determined from the thickness and the tributary width of the FRP composites, and can develop tensile stresses only. In this study, the constitutive relationship of the FRP truss element was assumed to be linear elastic behavior up to fracture.

Modeling of Bond Interface

The FRP composites are bonded to the concrete surface using bond materials such as epoxy. Accordingly, the modeling of the bond interface between the FRP and concrete surfaces is critically important to accurately simulating the contribution of the FRP composites to shear resistance. This study used the bond element to appropriately reflect the physical properties of the bond interface. Link elements and contact elements are two alternative elements commonly used to represent the bond element. The link element is a nondimensional element with two nodes, whereas the contact element is a linear-dimensional element with four nodes. The link element developed by Ngo and Scordelis (1967), as

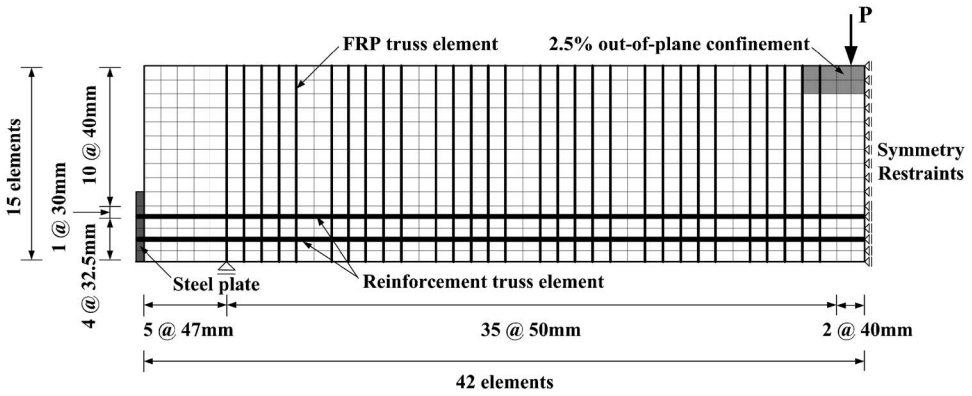

Fig. 3. FE representation of typical beam (RWOA-1)

shown in Fig. 2, was used in this research because it enables a variety of modeling approaches to be used by applying bond properties to each node.

In the FE mesh, the bond element is located between the concrete element and the FRP truss element. In the unloaded stage, the bond element exists between two nodes located on the same coordinate. However, when the load is applied, the nodes behave independently based on the response of the bond element. At this time, the bond stress-slip relationship is a most important factor in the behavior of the bond element. It depends on the compressive strength of concrete as well as the bond materials, such as the type of the FRP and the epoxy. This study used the following bilinear bond stress-slip relationship, proposed by Sato and Vecchio (2003), using the fracture energy of concrete G_f (Fig. 2):

$$\tau_{bFy} = (54f_c')^{0.19} \tag{1}$$

$$G_f = (\tau_{bFy}/6.6)^2 \tag{2}$$

$$s_{Fy} = 0.057G_f^{0.5} \tag{3}$$

$$s_{Fu} = 2G_f/\tau_{bFy} \tag{4}$$

where τ_{bFy}=maximum bond shear stress; f_c'=compressive strength of the concrete; s_{Fy}=bond slip at the maximum bond shear stress; and s_{Fu}=ultimate bond slip.

Verification Using Beams

To verify the proposed FE modeling methods for the FRP and bond interface, a total of four simply supported RC beams strengthened in shear with FRP composites were collected from the literature and compared with analytical results. Three beams tested by Wong and Vecchio (2003) had the same cross section, 305 mm width and 560 mm height, but different clear spans (3,660 mm, 4,570 mm, and 6,400 mm for beams RWOA-1, RWOA-2, and RWOA-3, respectively). The FRP strips of 200 mm width, spaced at 300 mm on center, were only bonded to the side of the RWOA series beams. On the other hand, the remaining beam, Beam2, tested by Sheikh et al. (2002) was wrapped with FRP sheets and had a width of 550 mm, height of 1,000 mm, and clear span of 3,850 mm. All the beams were subjected to three-point monotonic loading.

A FE mesh for the typical beam RWOA-1 is shown in Fig. 3. A VecTor2 analysis based on the DSFM was used for the numerical simulation. The bond stress-slip relationship, proposed by Sato and Vecchio (2003), and the link elements were used to model the bond interface between the FRP and the concrete. Table 1 gives the values of τ_{bFy}, s_{Fy}, and s_{Fu} for each compressive strength of concrete used in the beams. Additional details of the structural modeling were given by Wong and Vecchio (2003), who analyzed the beams using the MCFT and the contact elements. As shown in Fig. 4, the computed load-displacement responses successfully trace the observed ones with a mean of 0.98 and a coefficient of variation (COV) of 5.9% (Table 1). Although the numerical analysis somewhat underestimated the ductility of the beams, the resulting values are acceptable in terms of safety. Therefore, the indication from this study is that the proposed methods for the FE modeling of the FRP and the bond interface between the FRP and concrete are reasonably applicable to the FE analysis of the FRP-reinforced structures.

Table 1. Summary and Comparison of Experimental and Analytical Results for RC Beams

		Bond stress versus slip relationship			Maximum load		
Beam	f_c' (MPa)	τ_{bFy} (MPa)	s_{Fy} (mm)	s_{Fu} (mm)	Experimental (kN)	Analytical (kN)	*Ana./expt.*
RWOA-1	22.6	3.86	0.033	0.177	492.6	488.6	0.99
RWOA-2	25.9	3.96	0.034	0.182	458.7	474.6	1.03
RWOA-3	43.5	4.37	0.038	0.201	436.2	431.4	0.99
Beam2	45.7	4.41	0.038	0.203	2,528.0	2,266.9	0.90
Mean							0.98
COV							5.9%

Note: COV=Coefficient of variation.

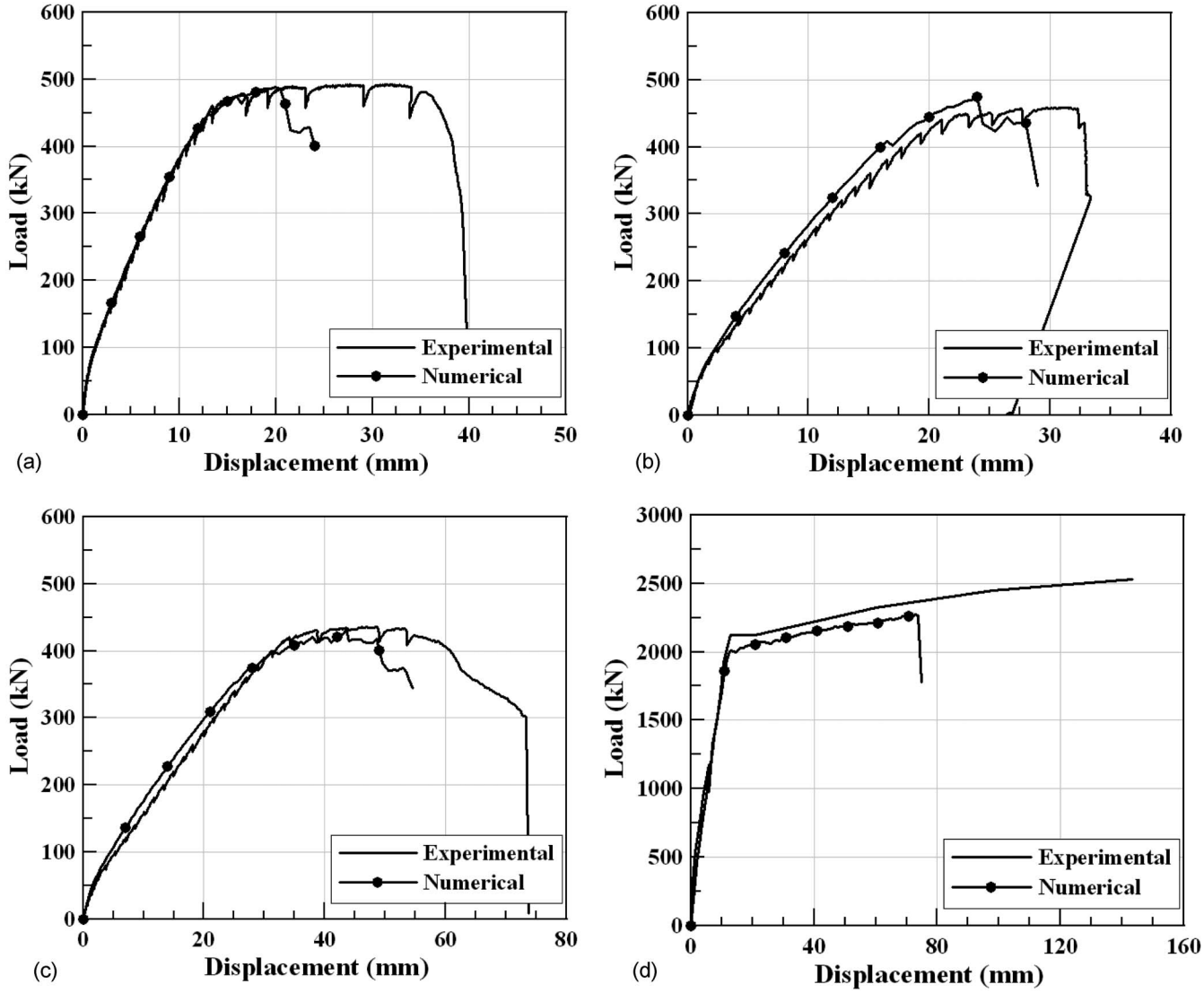

Fig. 4. Load-deflection relationships for RC beams with FRP composites: (a) RWOA-1; (b) RWOA-2; (c) RWOA-3; and (d) Beam2

Test of Shear-Critical RC Frame

Test Specimen Details

A shear-critical RC frame, which had member span-to-depth ratios, shear and longitudinal reinforcement ratios, and material strengths similar to those of the preheater tower structure previously described, was tested to verify the application of the DSFM. The maximum-size coarse aggregate used in the concrete was 10 mm. The average compressive strength of concrete at the time of the frame test was 43 MPa. No. 10, No. 20, and US No. 3 were used in the specimen, with yield strengths of 455, 447, and 506 MPa, respectively.

As shown in Fig. 5, the one-span two-story frame specimen had a height of 4.6 m and a width of 2.3 m. The width and depth of the beams and columns were 300 and 400 mm, respectively. For the fixed support condition, the specimen had a RC base with a width of 800 mm and thickness of 400 mm. The positions of the strain gauges bonded to the steel reinforcement within the specimen are illustrated in Fig. 5(a).

Carbon fiber-reinforced polymer (CFRP) composite wrap material was used to strengthen the frame after it had sustained extensive shear damage during Phase I testing (under monotonic lateral push-over loading). The CFRP wrap applied to the first- and second-story beams. The CFRP strips, 337.5 mm apart from center to center, had a width of 150 mm [Fig. 5(c)]. The deformations of all the CFRP strips were recorded by strain gauges with 60 mm length. The CFRP composite had carbon fibers and Kelvar 49 weft arranged in the longitudinal and transverse directions, respectively. From the results of standard coupon tests done according to ASTM D 3039, the tensile strength, elastic modulus, and ultimate strain of the fabric with an average thickness of 1.0 mm were 876 MPa, 72.4 GPa, and 12.1×10^{-3}, respectively.

Test Setup and Procedure

Shown in Fig. 6 is the test setup used to apply vertical and horizontal loads to the specimen. Variable horizontal load was applied to the frame at the midheight of the second-story beam. An axial load of 420 kN was applied to each column and maintained in a force-controlled manner during all phases of testing. Last, a stub

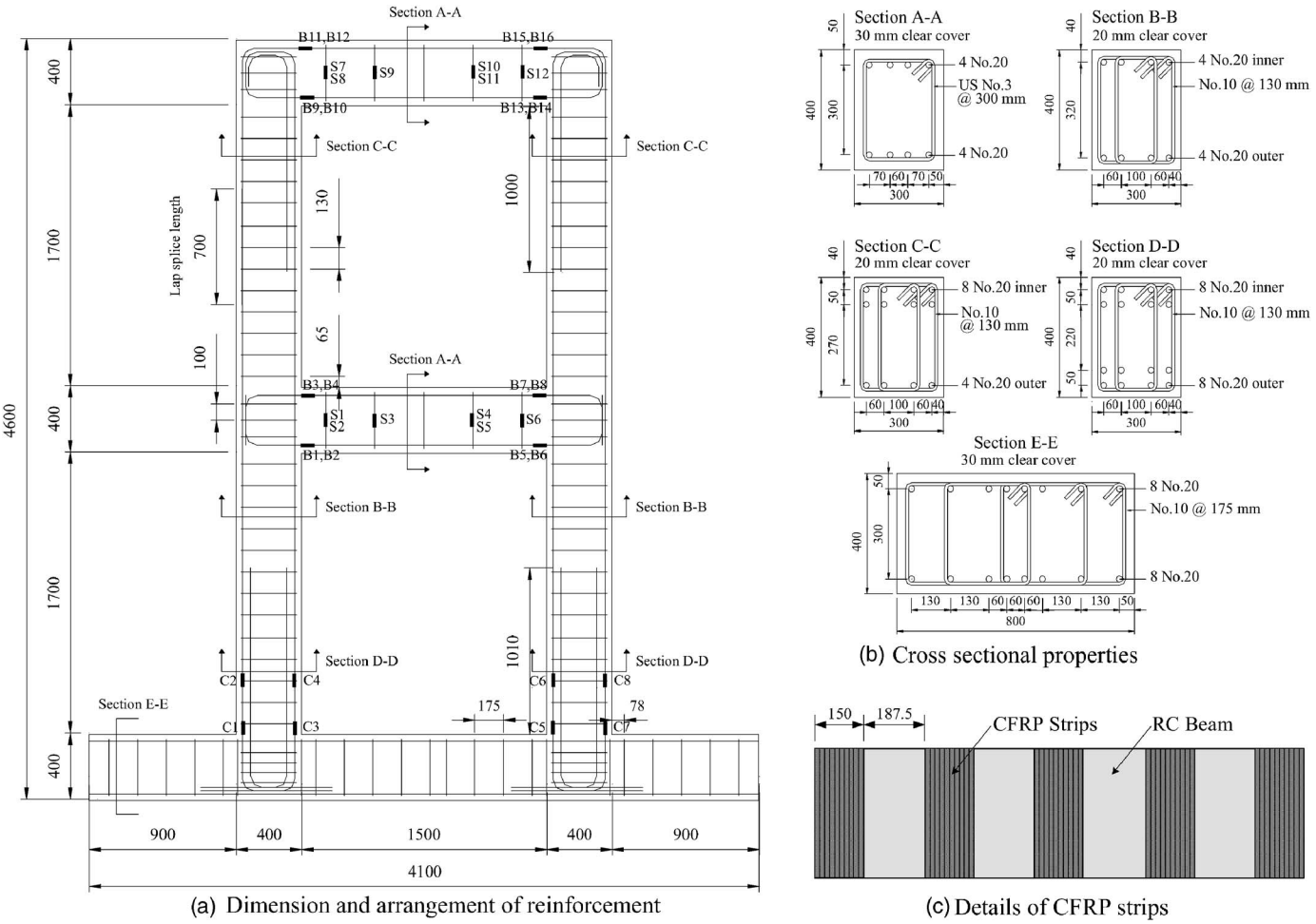

Fig. 5. Specimen details

steel beam was fastened to the top of each steel column for the purpose of out-of-plane support should twisting of the frame occur.

In the Phase I test, the specimen was subjected to a forward lateral drift of about 1.0% by which point significant shear damage had occurred in the beams and failure appeared imminent, and then it was returned up to zero displacement. Afterwards, a reverse load was applied to the specimen until it reached essentially the same displacement as in the forward cycle, and then again unloaded.

After the Phase I test was completed, the damaged concrete concentrated in the first- and second-story beams was repaired and the beams were strengthened with FRP strips [Fig. 5(c)]. During the repair phase, the axial load applied to each column was maintained at 420 kN. After the FRP strengthening of the specimen was completed, the Phase II testing was executed with displacement cycles of progressively increasing amplitude, as defined in Fig. 7. The yield displacement level (25 mm) used to define the drift levels was as experimentally measured in the Phase I test.

Phase I Test Results

The lateral load versus displacement response of the frame specimen obtained from Test Phase I is shown in Fig. 8(a). In the forward cycle, the applied maximum lateral load and the corresponding top-story lateral displacement were about 327 kN and 44.7 mm, respectively. The specimen showed a combined flexural-shear damage mode. The initial flexural yielding of the beam occurred almost simultaneously at both ends of the first-story beam at a force of 292 kN and corresponding displacement of 25 mm. The stirrup yielding was first observed in the first-story beam at a top-story displacement of 25.6 mm. After the shear reinforcement in the beams had yielded, severe shear cracks (with widths of up to 9 mm) developed along with the yielding of longitudinal reinforcements of the beams.

The maximum horizontal load applied to the specimen during Phase I was −304 kN, occurring during the reversed cycle and corresponding to a top-story displacement was −39.5 mm. The specimen sustained additional shear damage when loaded in the reverse direction. At no time, however, did the longitudinal bars of the columns yield as the maximum strain attained during Phase I test was 0.002.

Phase II Test Results

Shown in Fig. 8(b) is the lateral load-displacement response of the specimen obtained during Phase II testing. It can be seen that the behavior of the specimen was predominantly flexure controlled, owing to the FRP strengthening for shear. Furthermore, a full plastic hinge failure mechanism of the specimen was developed at the end of the Phase II test. The plastic hinges formed at all four beam ends and at both column bases. The maximum lateral load for the forward cycles was 421.5 kN at load cycle

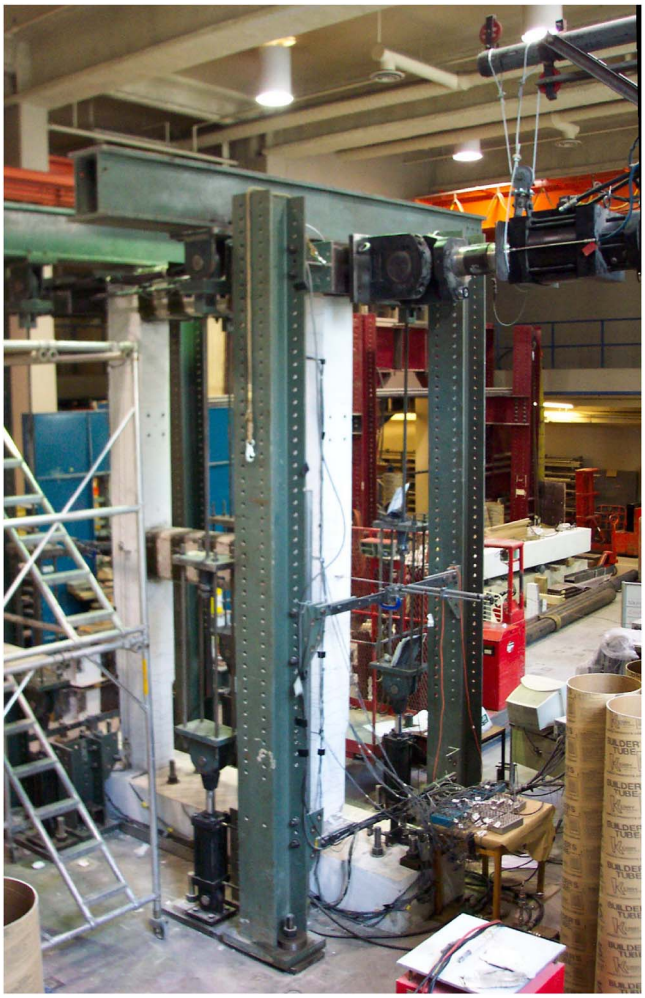

Fig. 6. Test setup of specimen

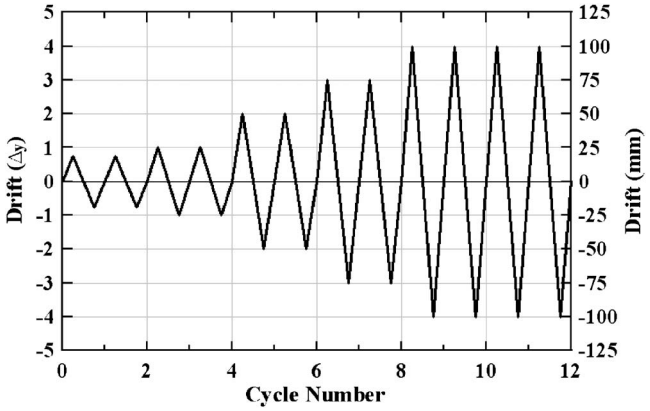

Fig. 7. Reversed cyclic loading history

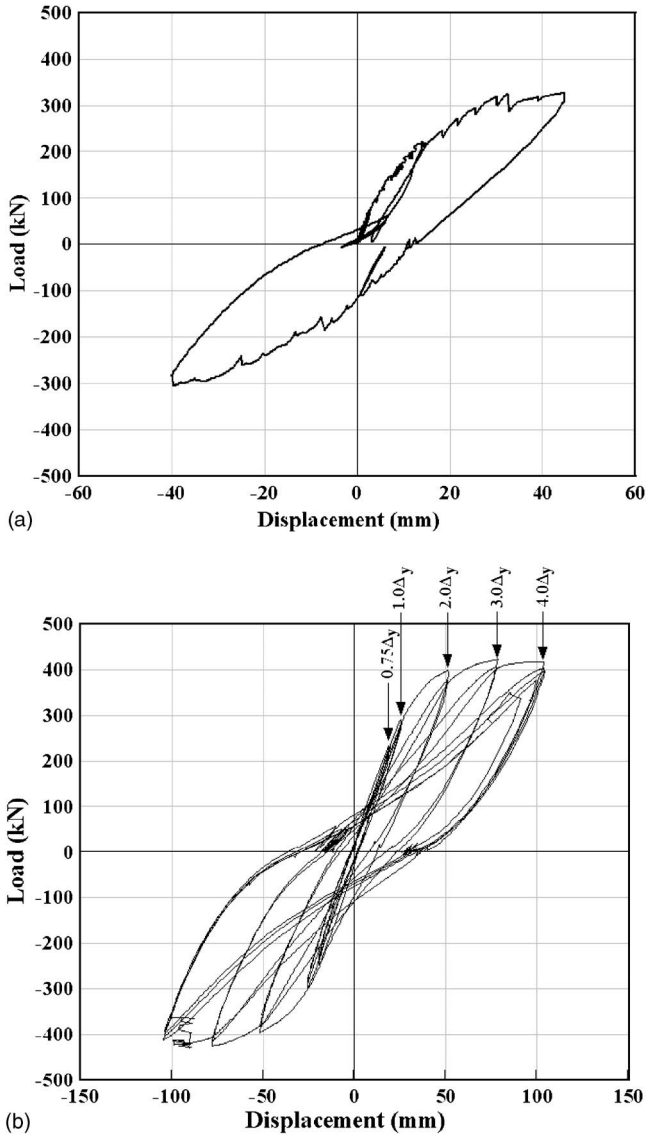

Fig. 8. Lateral load versus displacement responses of specimen: (a) Test Phase I; (b) Test Phase II

(LC) 7 ($+3.0\Delta_y$), and the corresponding displacement was about 78 mm. The maximum capacity of the specimen for the reverse cycles was also measured at LC7, and the peak load and displacement amounted to −424.4 kN and −77.4 mm, respectively.

The longitudinal bars of the first-story beam yielded at 269 kN, at a top-story displacement of 22.8 mm corresponding to LC3 ($+1.0\Delta_y$); those of the second-story beam yielded at 313 kN, at a top-story displacement of 29.1 mm corresponding to LC5 ($+2.0\Delta_y$). After yielding, the bars of the first- and second-story beams reached strain hardening at 324 kN of LC5 ($+2.0\Delta_y$) and −363 kN of LC5 ($-2.0\Delta_y$), respectively. In addition, at LC3 ($-1.0\Delta_y$) and LC5 ($-2.0\Delta_y$), all the longitudinal bars at the ends of the first- and second-story beams exhibited strain hardening response, respectively. First yielding of the longitudinal reinforcement at the base of the columns occurred at 369 kN corresponding to LC5 ($+2.0\Delta_y$); all longitudinal reinforcement at both column bases reached the yield strain at LC7 ($\pm 3.0\Delta_y$). Finally, the reinforcement at the base of the north column approached strain hardening at LC9 ($\pm 4.0\Delta_y$). Before the test was terminated, the concrete cover at the column bases had spalled.

The capacity of the frame decreased to 89% of the peak load under a total of four repeated loads from LC9 to LC12. Afterwards, while increasing the lateral load toward a target drift of $5.0\Delta_y$, the test was terminated due to out-of-plane distortion caused by the excessive damage of the two beams at 349.4 kN.

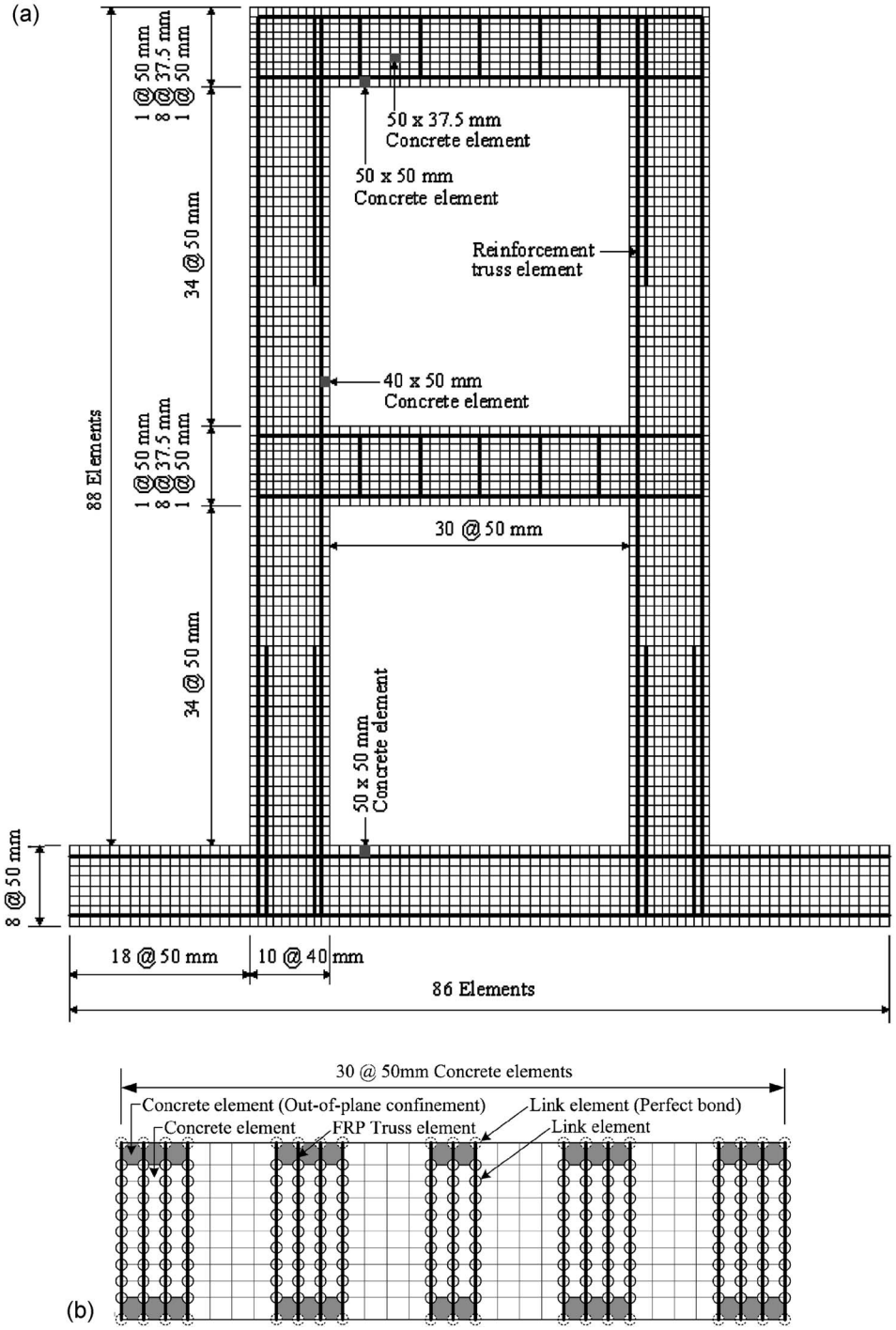

Fig. 9. FE modeling of RC frame with FRP strips: (a) RC frame; (b) FRP strips wrapped around a beam

Although premature failure occurred, it should be noted that fully developed plastic hinges had formed at every beam end and at each column base of the specimen.

Because 50% of each beam was wrapped with the FRP strips, it was not possible to observe the nature of the cracks that formed under the strips. In particular, the maximum width of the flexural crack could not be measured because CFRP strips were located at the ends of the beams up to the face of the columns. Although fully developed flexural plastic hinges were formed at all joint and support locations within the frame, shear also influenced the behavior of the beams. However, it was difficult to analyze the effect of shear from the deformation of the stirrups, because almost half of the strain gauges attached to the stirrups became nonfunctional due to the excessive strains sustained during the Phase I test.

The shear cracks, observed at locations along each beam where FRP strips were not present, were about 1.5 mm in width at a drift target of $\pm 3.0\Delta_y$ and developed up to a width of 2.5 mm at $\pm 4.0\Delta_y$. Although the shear cracks had a large width, they were relatively smaller than the flexural crack widths. In addition, fracture of the FRP strips was not observed anywhere. While the majority of the FRP strains at the first-story beam ranged from 0.003 to 0.0055, those at the second-story beam were 0.003 or less.

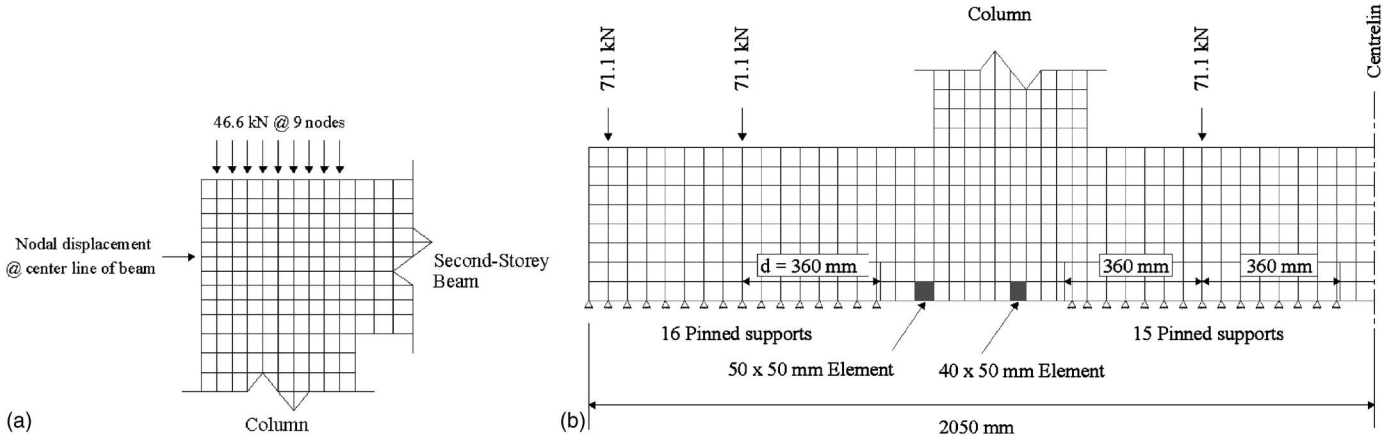

Fig. 10. Details of structural modeling: (a) lateral and axial load conditions; (b) base support condition

A more complete discussion of the details and results of the frame test is provided by Duong et al. (2007).

Modeling of Test Frame

The theoretical behavior of the CFRP-repaired test frame was determined using the two-dimensional nonlinear FE analysis program VecTor2 based on the DSFM. In addition, the program FormWorks (Wong and Vecchio 2002), an advanced graphics-based preprocessor for VecTor2, was used in developing the FE model for the frame specimen.

Modeling of Reinforced Concrete

A total of 3,048 quadrilateral elements were used for modeling the concrete members. As can be shown in Fig. 9(a), the width and height of concrete elements were selected in consideration of the sizes of members and the locations of steel bars. The thickness of the concrete elements was the same as that of the frame specimen. The concrete elements in the base and columns had single thicknesses of 800 and 300 mm, respectively, whereas the beams had two kinds of thickness, 300 and 225 mm. The thickness of 225 mm was applied to the elements at the top and bottom of the beams in consideration of rounding off the beam cover for wrapping the FRP strips. Furthermore, the out-of-plane confinement by the FRP wrapping was considered in the elements at the top and bottom of the beams where the FRP strips were bonded, as shown in Fig. 9(b).

The default models designated in VecTor2 were used unless there was a valid reason to select an alternative model. The details of the constitutive models and their implementation into the FE program have been reported elsewhere (Wong and Vecchio 2002) exclusive of Montoya model (Montoya 2003). The Popovics (HSC) model was selected for the compression prepeak response of concrete to more accurately represent the response of the high strength concrete used in this specimen. The most recently developed models, Montoya model (Montoya 2003) and Palermo model (Palermo and Vecchio 2002), were used for the concrete compression postpeak relationship and the concrete hysteretic response, respectively. The bilinear model was selected to consider the effect of the tension softening of concrete.

The transverse reinforcement in the base and columns were included in the concrete elements as smeared reinforcement. However, all longitudinal reinforcement within the base, columns, and beams, and all stirrups within the beams, was modeled discretely using truss bar elements connected directly to the concrete elements. A total of 986 truss elements were used for the modeling of the steel reinforcement. The behavior of the reinforcing bars was assumed to be elastic plastic with the strain hardening effects; the Bauschinger effect was included in the cyclic modeling.

Every steel bar used in the specimen had an adequate development length. Therefore, the ends of the steel bars with hooks were assumed to have a perfect bond rather than modeling the bar hooks. However, the cross-sectional area of the steel bars, in which the development length was accomplished by straight steel bars, was decreased in approximate proportion to the decreasing steel stress over the development length. This was done in order to consider the gradually decreasing stress within the reinforcing bars approaching bar ends. For example, the development length required by ACI 318-05 Code (ACI Committee 318 2005) was calculated as approximately 600 mm for the No. 20 straight bars anchored in the column. Accordingly, the cross-sectional area of the truss elements used to represent these bars was gradually decreased over a distance starting 600 mm from the ends of the bars.

FRP and Bond Modeling

A total of 380 truss elements were used to model the FRP strips, and their constitutive response was modeled as linear elastic up to fracture. Fig. 9(b) shows the modeling of the FRP strips wrapped around a beam. The FRP strip was modeled with truss elements along three or four nodal grid lines, depending on the width of the concrete elements. It should be noted that all the FRP strips in the FE mesh had the same bonded-surface and cross-sectional areas.

The truss elements representing the FRP strip were indirectly attached to the underlying concrete elements via bond-link element. The bond stress versus slip relationship of the bond elements was as obtained from Eqs. (1)–(4). For the concrete compressive strength of 43 MPa, τ_{bFy}, G_f, s_{Fy}, and s_{Fu} were 4.36 MPa, 0.436 N/mm, 0.038, and 0.2 mm, respectively. Since the FRP strips were wrapped around the beams in the test frame, it can be assumed that the FRP strips at the beam corners were perfectly bonded to the concrete surfaces. To consider this characteristic, an arbitrarily high bond strength was applied to the bond elements located in the beam corners, as shown in Fig. 9(b). The bond area was calculated according to the tributary area of the FRP strips around the bond element.

Structural Modeling

Three types of load cases were used for the numerical analysis of the frame. As seen in Fig. 10(a), Load Case I represented the lateral load applied at the middle of the second-story beam at the pushing end. In the FE analysis, the lateral load was controlled so that the nodal displacement continually increased by 1 mm increments. To account for the axial loads applied to the columns and the posttensioning forces applied to the base, the corresponding nodal loads were modeled as Load Case II. A vertical load of 420 kN, uniformly applied to each column via loading plates in the test, was distributed to 9 column nodes; in other words, 46.67 kN was applied to each column node, as illustrated in Fig. 10(a). Furthermore, because the testing of the frame specimen began approximately 9 months after casting, the frame specimen was influenced by drying shrinkage. Therefore, a shrinkage strain of −0.0004 was applied to every concrete element within the frame; this constituted Load Case III.

To provide the fixed end condition of the frame, the frame base was posttensioned onto the strong floor by six sets of floor bolts in this test. One set consisted of two bolts and was stressed to about 71 kN. In the FE analysis, these posttensioning forces were modeled as six downward forces of 71 kN at the bolt locations, as shown in Fig. 10(b). The pinned support condition was applied to the bottom of the frame base within a distance of d from each bolt location, where d=effective depth of the base. No base slip in the test indicated that the pinned support condition was reasonable.

Comparison of Numerical and Experimental Results

Test Phase I Response

Shown in Fig. 11(a), for the lateral load-displacement response of the RC frame without FRP composites, is a comparison between the experiment-observed behavior and the numerical analysis results obtained from VecTor2. The calculated load-displacement curve for the forward cycle shows reasonable agreement with the experimental results. The computed peak-load and the corresponding displacement were 356.3 kN and 44 mm, respectively, which translate to calculated-to-experiment ratios of 1.09 and 0.98 for the peak-load and displacement, respectively. In the FE analysis, the first yielding of the longitudinal bars and stirrups occurred in the first-story beam, and the computed lateral force and displacement were 232.5 kN and 19 mm, and 249.8 kN and 21 mm, respectively. It was similar to the test result that both steel bars yielded at almost the same time, but the values were somewhat premature compared to the experimentally recorded displacement of about 25 mm.

For the reverse cycle, the FE analysis resulted in the peak load of −333.4 kN, which was in 9.7% error of the experimental result of −304 kN. The calculated energy dissipation capacity, taken as the area enclosed by the load-displacement curve, of the reverse cycle was smaller than that of the experimental result. This is because the force of restoration of the frame damaged in shear was more or less overestimated in the FE analysis. With regard to this, further research should be conducted.

Test Phase II Response

Fig. 11(b) illustrates the comparison between the experimental and numerical lateral load-displacement responses for the frame

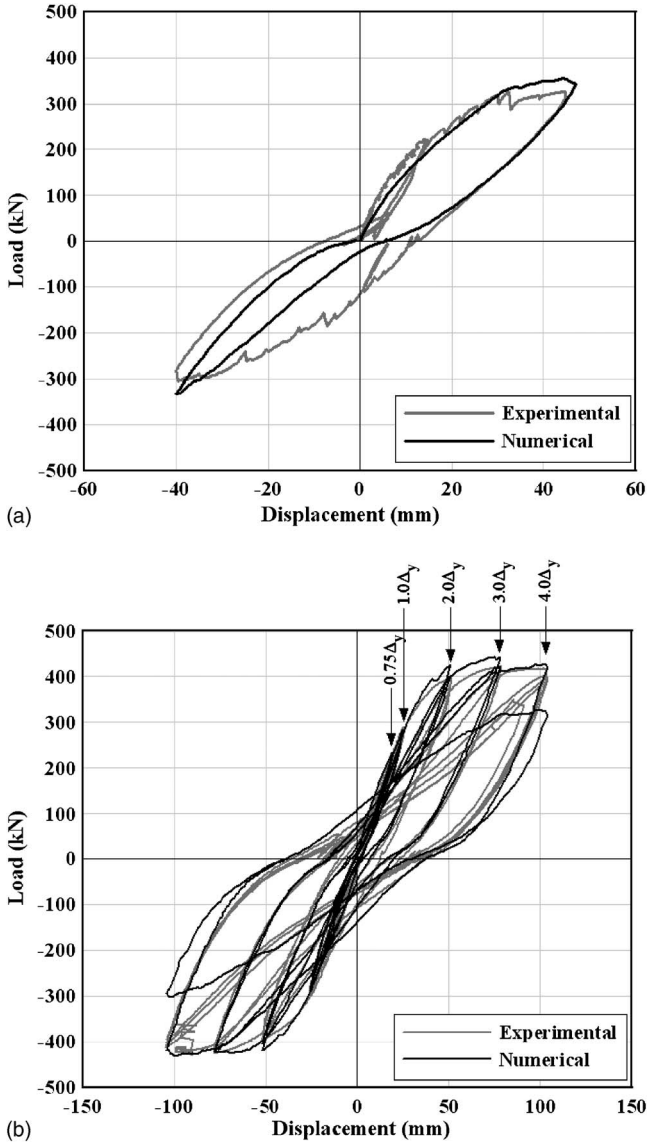

Fig. 11. Comparison of experimental and analytical results for lateral load versus displacement relationship of frame specimen: (a) Test Phase I; (b) Test Phase II

strengthened in shear with FRP strips. It can be seen that the predicted response was in excellent agreement with the experimental behavior. In addition, the lateral load-displacement response obtained from the FE analysis illustrates that the frame was primarily governed by flexure. This result indicates that the FRP strips effectively controlled the shear cracks, preventing a shear-dominant failure mechanism and a sudden reduction of the frame capacity. In the numerical analysis, the frame strength fell to less than 80% of the peak load at LC10 ($\pm 4.0\Delta_y$), where Δ_y refers to the initial yielding of the frame obtained from Phase I testing.

Table 2 compares the computed and measured results of the maximum load and the corresponding displacement for each load cycle up to LC9 ($\pm 4.0\Delta_y$), which is just before the failure of the frame in the analysis. As illustrated by this table, the proposed FE analysis has a good accuracy with not only a mean of 1.01 and a COV of 4.1% for the maximum load, but also 0.99 and 2.9% for the displacement.

Shown in Fig. 12(a) is the predicted crack pattern for the entire

Table 2. Comparison of Computed and Measured Results at Peak Load for Each Load Cycle

		Load (kN)			Displacement (mm)		
Cycle	Drift (Δ_y)	Analytical	Experimental	*Ana./expt.*	Analytical	Experimental	*Ana./expt.*
1	+0.75	233.7	232.9	1.00	19.0	18.8	1.01
	−0.75	−229.1	−247.2	0.93	−19.0	−19.2	0.99
2	+0.75	226.4	233.5	0.97	19.0	19.3	0.98
	−0.75	−227.9	−241.1	0.95	−19.0	−19.6	0.97
3	+1.0	284.6	291.4	0.98	25.0	25.2	0.99
	−1.0	−292.5	−297.9	0.98	−26.0	−25.7	1.01
4	+1.0	277.8	283.2	0.98	25.0	25.4	0.98
	−1.0	−286.6	−288.6	0.99	−26.0	−25.7	1.01
5	+2.0	425.8	398.8	1.07	51.0	51.1	1.00
	−2.0	−418.2	−395.4	1.06	−52.0	−51.7	1.01
6	+2.0	401.8	377.0	1.07	51.0	51.1	1.00
	−2.0	−403.4	−383.6	1.05	−52.0	−51.5	1.01
7	+3.0	441.7	421.5	1.05	75.0	77.9	0.96
	−3.0	−425.8	−424.4	1.00	−69.0	−77.4	0.89
8	+3.0	420.2	406.3	1.03	77.0	77.6	0.99
	−3.0	−419.7	−413.9	1.01	−78.0	−77.7	1.00
9	+4.0	431.8	416.8	1.04	102.0	103.6	0.98
	−4.0	−431.9	−422.1	1.02	−99.0	−98.5	1.01
Mean				1.01			0.99
COV				4.1%			2.9%

frame as obtained from the FE analysis. The analysis indicated flexural plastic hinges forming at the ends of the beams and at the column bases, but with significant shear cracks also developing in the beams near the column joints; these outcomes are consistent with the test results. Fig. 12(b) shows the experimental and analytical crack patterns of the first-story beam, which sustained the greatest damage. Although it is difficult to compare the crack patterns of the beam due to the overlying FRP wrap, it can be seen that the predicted crack pattern is very similar to the observed one.

The analysis indicated that the initial flexural yielding of the first-story beam occurred at a load of 284.5 kN and corresponding top-story displacement of 25 mm, occurring at Load Stage LC3 ($+1.0\Delta_y$). This result corresponds to errors of about 6 and 10% for the observed lateral load (269 kN) and the displacement (22.8 mm), respectively. The numerical analysis predicted that the first flexural yielding of the second-story beam occurred at LC5 ($+2.0\Delta_y$), and that all the longitudinal bars in the lower and upper beams and the columns yielded at LC3 ($-1.0\Delta_y$), LC5 ($-2.0\Delta_y$), and LC7 ($+3.0\Delta_y$), respectively, again consistent with the observed results. However, some difference existed between the analytical and experimental results with respect to the initial yielding of the column. In the experiment, it was observed to occur at LC5 ($+2.0\Delta_y$) whereas, in the FE Analysis, it was predicted at LC5 ($-2.0\Delta_y$).

It was difficult to collect reliable experimental data from the strain gauges attached to the stirrups after the completion of Phase I testing due to excessive damage; hence, verification of the accuracy of the FE analysis with regard to the shear deformation of the frame was sought from the straining of the CFRP strips. Table 3 compares the observed and calculated maximum strains in the CFRP strips (at midheight) for typical forward cycles. The observed and predicted maximum strains in the CFRP wrap occurred in a strip bonded near the shear-critical section of the first-story beam. The FE analysis results were in good agreement with the experimental results, with a mean of 1.02 and a COV of 7.6%. In addition, there was no fracture of the FRP strips in the analysis, which was consistent with the observed result. Therefore, the proposed numerical modeling method can be reasonably used for analyzing the shear-strengthened RC frame with FRP composites.

Current code provisions suggest that, under seismic load conditions, no shear strength contribution should be ascribed to the concrete; that is, influences from concrete tension stiffening and aggregate interlock mechanisms should be neglected. Fig. 13 compares the experimental and predicted load-displacement responses, where the theoretical result did not take into account the concrete tensile strength-related mechanisms. It is worth noting that the computed result significantly underestimated the energy dissipation and effective stiffness of the strengthened frame, although the ultimate strength was little affected. This suggests that even if the concrete is previously damaged in shear, the tensile strength of repaired concrete and the tension stiffening response of FRP-confined concrete should be considered. Further studies are required for the postpeak behavior of the frame with FRP composites under cyclic load.

Conclusions

This study demonstrated that accurate simulations of the response of FRP-strengthened shear-critical concrete frame structures can be obtained from finite-element-based models and analysis procedures. In particular, the prediction capacity of the DSFM was verified. Various numerical FE modeling methods applicable to FRP-strengthened concrete frame structures were proposed, and their accuracy were confirmed through comparisons with experimental results of a large-scale frame test specimen. The following conclusions are drawn from this research:

1. Nonlinear finite-elementt analysis tools, such as program

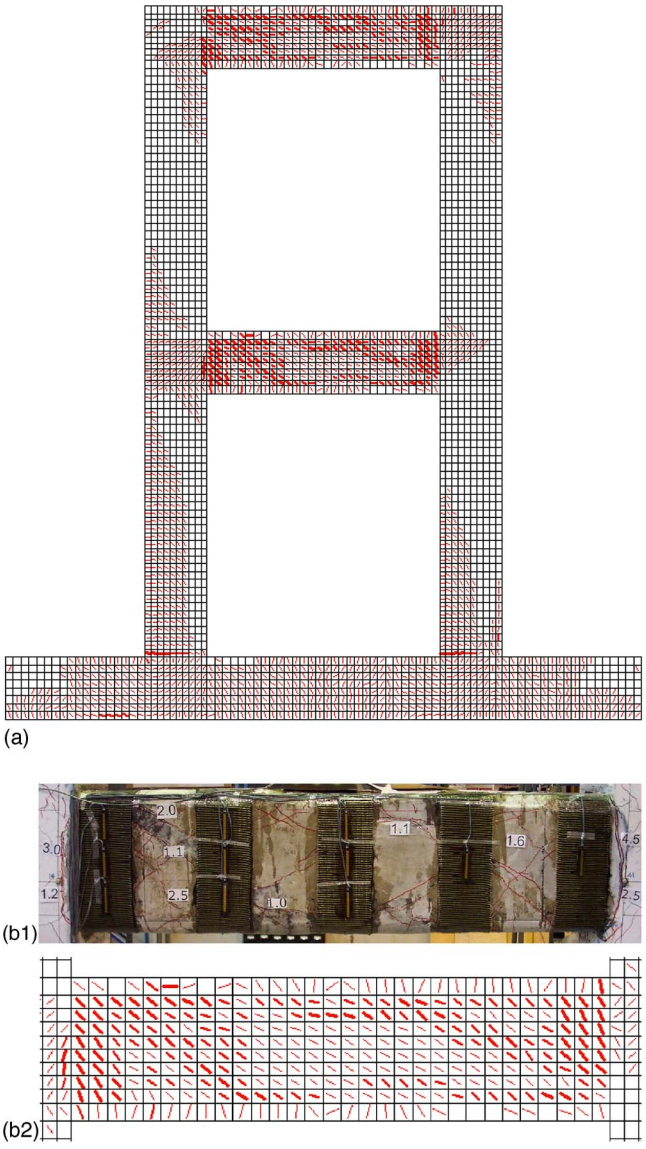

Fig. 12. Predicted and experimental crack patterns for Test Phase II at LC9 (+4.0Δ_y): (a) frame; (b) first-story beam

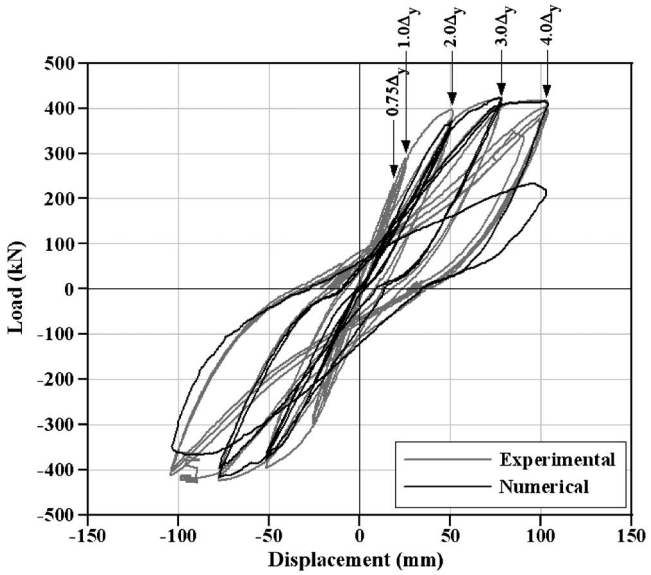

Fig. 13. Comparison of observed and predicted lateral load versus displacement responses without considering tensile strength of concrete

Table 3. Comparison of Observed and Analytical Maximum Strains in CFRP Wrap

Cycle	Drift (Δ_y)	$\varepsilon_{f,\text{exp}}$ ($\times 10^{-3}$)	$\varepsilon_{f,\text{ana}}$ ($\times 10^{-3}$)	$\frac{\varepsilon_{f,\text{ana}}}{\varepsilon_{f,\text{exp}}}$
1	+0.75	1.31	1.16	0.89
2	+0.75	1.46	1.32	0.90
3	+1.0	1.88	2.07	1.10
4	+1.0	2.11	2.18	1.03
5	+2.0	3.17	3.41	1.08
6	+2.0	3.77	3.87	1.03
7	+3.0	3.85	4.04	1.05
8	+3.0	4.46	4.45	1.00
9	+4.0	4.55	4.95	1.09
Mean				1.02
COV				7.6%

VecTor2 based on the DSFM, can be used to reasonably accurately predict the response of concrete frames shear strengthened with FRP composites.

2. The proposed numerical modeling methods were successfully used to predict the constitutive states, as well as the damage mode, crack pattern, and hysteretic behavior of a frame strengthened with FRP composites. In particular, the proposed methods for the FE modeling of the FRP and the bond interface between the FRP and concrete provided a good correlation to experimentally observed responses.
3. Although a frame may have been previously damaged in shear, once it has been repaired and strengthened, the tensile strength of the repaired concrete and the tension stiffening response of FRP-confined concrete should be considered for improved accuracy in predicted response up to peak load.

Acknowledgments

This work was supported by the Korea Research Foundation Grant No. KRF-2005-214-D00177. Their support is gratefully acknowledged. The writers wish to express their sincere gratitude to Professor Yuichi Sato of Kyoto University in Japan for his discussions and Professor Jung-Yoon Lee of Sungkyunkwan University in South Korea for providing the opportunity of this research.

References

ACI Committee 318. (2005). "Building code requirements for structural concrete (ACI 318-05) and commentary." *ACI 318-05* and *318R-05*, American Concrete Institute, Farmington Hills, Mich.

Al-Sulaimani, G. J., Sharif, A. M., Basunbul, I. A., Baluch, M. H., and Ghaleb, B. N. (1994). "Shear repair for reinforced concrete by fibreglass plate bonding." *ACI Struct. J.*, 91(4), 458–464.

Berset, J.-D (1992). "Strengthening of reinforced concrete beams for shear using FRP composites." MS thesis, Dept. of Civil and Environmental Engineering, Massachusetts Institute of Technology.

Bousselham, A., and Chaallal, O. (2004). "Shear strengthening reinforced

concrete beams with fiber-reinforced polymer: Assessment of influencing parameters and required research." *ACI Struct. J.*, 101(2), 219–227.

Bousselham, A., and Chaallal, O. (2006). "Behavior of reinforced concrete T-beams strengthened in shear with carbon fiber-reinforced polymer—An experimental study." *ACI Struct. J.*, 103(3), 339–347.

Chaallal, O., Nollet, M. J., and Perraton, D. (1998). "Shear strengthening of RC beams by externally bonded side CFRP strips." *J. Compos. Constr.*, 2(2), 111–113.

Chajes, M. J., Januszka, T. F., Mertz, D. R., Thomson, T. A., and Finch, W. W. (1995). "Shear strengthening of reinforced concrete beams using externally applied composite fabrics." *ACI Struct. J.*, 92(3), 295–303.

Chen, J. F., and Teng, J. G. (2003). "Shear capacity of fiber-reinforced polymer-strengthened reinforced concrete beams: Fiber reinforced polymer rupture." *J. Struct. Eng.*, 129(5), 615–625.

Duong, K. V., Sheikh, S. A., and Vecchio, F. J. (2007). "Seismic behavior of shear-critical reinforced concrete frame: Experimental investigation." *ACI Struct. J.*, 104(3), 303–310.

Khalifa, A., Gold, W. J., Nanni, A., and Abdel-Aziz, M. I. (1998). "Contribution of externally bonded FRP to shear capacity of RC flexural member." *J. Compos. Constr.*, 2(4), 195–202.

Li, A., Dagana, C., and Delmas, Y. (2001). "CFRP contribution to shear capacity of strengthened RC beams." *Eng. Struct.*, 23(10), 1212–1220.

Montoya, E. (2003). "Behavior and analysis of confined concrete." Ph.D. thesis, Univ. of Toronto, Toronto, Canada.

Ngo, D., and Scordelis, A. C. (1967). "Finite-element analysis of reinforced concrete beams." *ACI J.*, 64(3), 152–163.

Norris, T., Sindatmanesh, H., and Ehsani, M. R. (1997). "Shear and flexural strengthening of R/C beams with carbon fiber sheets." *J. Struct. Eng.*, 123(7), 903–911.

Palermo, D., and Vecchio, F. J. (2002). "Behavior and analysis of reinforced concrete walls subjected to reversed cyclic loading." *Publication No. 2002–1*, Dept. of Civil Engineering, Univ. of Toronto, Toronto, Canada.

Pellegrino, C., and Modena, C. (2002). "Fiber reinforced polymer shear strengthening of reinforced concrete beams with transverse steel reinforcement." *J. Compos. Constr.*, 6(2), 104–111.

Pellegrino, C., and Modena, C. (2006). "Fiber-reinforced polymer shear strengthening of reinforced concrete beams: Experimental study and analytical modeling." *ACI Struct. J.*, 103(5), 720–728.

Saadatmanesh, H., and Ehsani, M. R. (1990). "Fiber composite plates can strengthen beams." *Concr. Int.*, 12(3), 65–71.

Sato, Y., and Vecchio, F. J. (2003). "Tension stiffening and crack formation in reinforced concrete members with fiber-reinforced polymer sheets." *J. Struct. Eng.*, 129(6), 717–724.

Sheikh, S. A., DeRose, D., and Mardukhi, J. (2002). "Retrofitting of concrete structures for shear and flexure with fiber-reinforced polymers." *ACI Struct. J.*, 99(4), 451–459.

Triantafillou, T. C. (1998). "Shear strengthening of reinforced concrete beams using epoxy-bonded FRP composites." *ACI Struct. J.*, 95(2), 107–115.

Triantafillou, T. C., and Antonopoulos, C. P. (2000). "Design of concrete flexural members strengthened in shear with FRP." *J. Compos. Constr.*, 4(4), 198–205.

Vecchio, F. J. (2000). "Disturbed stress field model for reinforced concrete: Formulation." *J. Struct. Eng.*, 126(9), 1070–1077.

Vecchio, F. J., and Collins, M. P. (1986). "The modified compression field theory for reinforced concrete elements subjected to shear." *ACI J.*, 83(2), 219–231.

Wong, P. S., and Vecchio, F. J. (2002). "VecTor2 and FormWorks user's manual." *Technical Rep.*, Dept. of Civil Engineering, Univ. of Toronto, Toronto, Canada, ⟨http://www.civ.utoronto.ca/vector/⟩.

Wong, R. S. Y., and Vecchio, F. J. (2003). "Towards modeling of reinforced concrete members with externally bonded fiber-reinforced polymer composites." *ACI Struct. J.*, 100(1), 47–55.